AD-A057 403 OHIO STATE UNIV COLUMBUS ELECTROSCIENCE LAB F/G 20/3
NEAR FIELDS OF A VECTOR ELECTRIC LINE SOURCE NEAR THE EDGE OF A--ETC(U)
JUN 78 D M POZAR, E H NEWMAN DAAG29-76-G-0331
UNCLASSIFIED ESL-784569-5 ARO-14012.2-EL NL

| OF |
AD
A057403

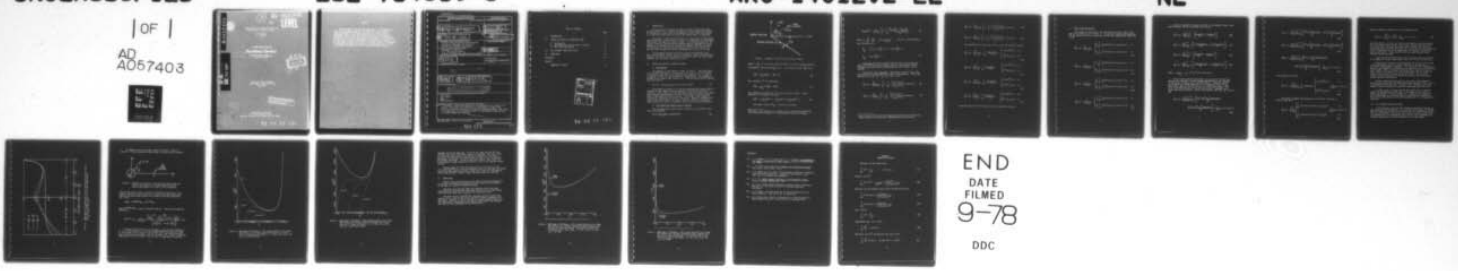

END
DATE
FILMED
9-78
DDC

ElectroScience Laboratory

Department of Electrical Engineering
Columbus, Ohio 43212

Technical Report 784569-5
Grant Number DAAG29-76-G-0331
June 1978

UNCLASSIFIED

SECURITY CLASSIFICATION OF THIS PAGE *(When Data Entered)*

REPORT DOCUMENTATION PAGE		READ INSTRUCTIONS BEFORE COMPLETING FORM
1. REPORT NUMBER	2. GOVT ACCESSION NO.	3. RECIPIENT'S CATALOG NUMBER
4. TITLE *(and Subtitle)* (6) NEAR FIELDS OF A VECTOR ELECTRIC LINE SOURCE NEAR THE EDGE OF A WEDGE.		5. TYPE OF REPORT & PERIOD COVERED (9) Technical report;
		6. PERFORMING ORG. REPORT NUMBER (14) ESL-784569-5
7. AUTHOR(s) (10) D. M. Pozar and E. H. Newman		8. CONTRACT OR GRANT NUMBER(s) (15) Grant No. DAAG29-76-G-0331
9. PERFORMING ORGANIZATION NAME AND ADDRESS The Ohio State University ElectroScience Laboratory, Department of Electrical Engineering, Columbus, Ohio 43212		10. PROGRAM ELEMENT, PROJECT, TASK AREA & WORK UNIT NUMBERS
11. CONTROLLING OFFICE NAME AND ADDRESS Department of the Army U. S. Army Research Office Research Triangle Park, North Carolina 27709		(11) 12. REPORT DATE June 1978
		13. NUMBER OF PAGES 17
14. MONITORING AGENCY NAME & ADDRESS *(if different from Controlling Office)* (12) 21 p.		15. SECURITY CLASS. *(of this report)* Unclassified
		15a. DECLASSIFICATION/DOWNGRADING SCHEDULE

16. DISTRIBUTION STATEMENT *(of this Report)*

Approved for public release; distribution unlimited.

17. DISTRIBUTION STATEMENT *(of the abstract entered in Block 20, if different from Report)*

(18) ARO (19) 14012.2-EL

18. SUPPLEMENTARY NOTES

THE VIEW, OPINIONS, AND/OR FINDINGS CONTAINED IN THIS REPORT ARE THOSE OF THE AUTHOR(S) AND SHOULD NOT BE CONSTRUED AS AN OFFICIAL DEPARTMENT OF THE ARMY POSITION, POLICY, OR DECISION, UNLESS SO DESIGNATED BY OTHER DOCUMENTATION.

19. KEY WORDS *(Continue on reverse side if necessary and identify by block number)*

Near fields
Line source
Wedge
Edge condition

20. ABSTRACT *(Continue on reverse side if necessary and identify by block number)*

Simple, closed form expressions are obtained for the fields of an electric line source with transverse or longitudinal current flow, parallel to and near the edge of a perfectly conducting wedge. The effect of an edge which is not perfectly sharp is investigated by considering a cylinder-tipped half-plane.

DD FORM 1 JAN 73 1473 EDITION OF 1 NOV 65 IS OBSOLETE

UNCLASSIFIED

SECURITY CLASSIFICATION OF THIS PAGE *(When Data Entered)*

402 251

TABLE OF CONTENTS

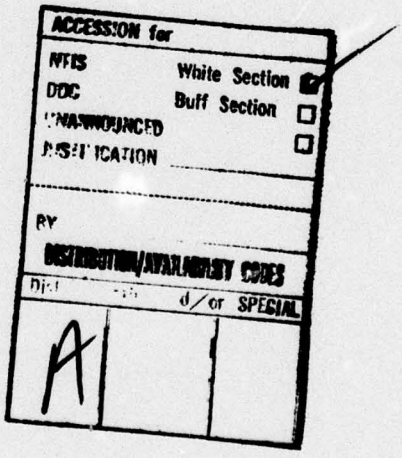

I. INTRODUCTION

The problem of scattering by wedges has been treated extensively by many authors [1,2]. Usually the analysis involves asymptotic methods to evaluate far-fields, with little emphasis on near-field calculations. It is the near-field aspect with which the present paper is concerned.

An interest in the near zone fields of a source near an edge arises when formulating a moment method solution to the problem of a wire antenna mounted near the edge of a plate or wedge. In a previous paper [3], the authors presented a moment method technique whereby problems with wires mounted .1λ or greater from an edge may be treated. Desiring to extend this technique by synthesizing an expansion mode to treat the case of the wire near an edge, the analysis presented here forms a first step.

In the present analysis an electric line source parallel to an edge, with arbitrary current flow, is considered. Simple expressions for the near zone fields are derived which exhibit not only the correct edge behavior, but the source singularity as well.

II. THEORY FOR PERFECTLY CONDUCTING WEDGE

A. Introduction

The geometry of the problem is shown in Figure 1. The field point is (ρ,ϕ) while the electric line source is at (ρ',ϕ'). The line source is parallel to the edge of the wedge and has components I_ρ, I_ϕ, and I_z of current in the $\hat{\rho}$, $\hat{\phi}$, and $\hat{z}$ directions, respectively. The current is assumed to be constant with respect to z. Thus the source current density may be written as

$$\bar{J}(\rho,\phi) = (I_\rho\hat{\rho}+I_\phi\hat{\phi}+I_z\hat{z})\,\frac{1}{\rho}\,\delta(\rho-\rho')\delta(\phi-\phi')\ A/M^2. \tag{1}$$

The method of solution is to use the two-dimensional dyadic Green's function for the wedge to find the magnetic field due to the vector current $\bar{J}$. Then, since the field and source points are close to the edge, small argument approximations are used for the Bessel functions which occur in the resulting infinite series. The series is then summed in closed form, preserving the source singularity. Maxwell's equations are used to find the $\bar{E}$ fields. Of course, with the fields of an electric source known, the fields of a magnetic source may be found from duality.

B. Two-Dimensional Dyadic Green's Function

The two-dimensional dyadic Green's function is a solution of the vector wave equation

$$(\nabla x\nabla x-k^2)\bar{\bar{G}}_{m2}(\bar{R}|\bar{R}')=\nabla x[\bar{\bar{I}}\delta(\bar{R}-\bar{R}')] \tag{2}$$

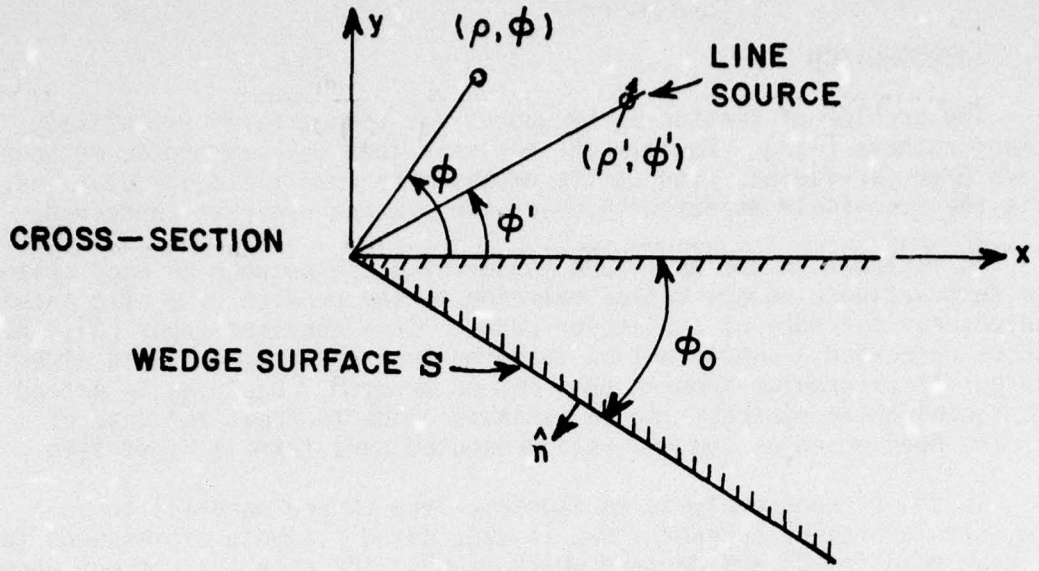

Figure 1. Geometry of the line source near an edge.

where $k = \frac{2\pi}{\lambda_o}$, $\bar{\bar{I}}$ is the unit dyad, $\bar{R}=\rho\hat{\rho}+\phi\hat{\phi}$, $\bar{R}'=\rho'\hat{\rho}+\phi'\hat{\phi}$, and $\bar{\bar{G}}_{m2}$ satisfies the boundary condition $\hat{n}x\nabla x\bar{\bar{G}}_{m2}=0$ on s. The fields are then found from

$$\bar{H}(\bar{R}) = \int \bar{\bar{G}}_{m2}(\bar{R}|\bar{R}') \cdot \bar{J}(\bar{R}')\, ds, \tag{3}$$

and, assuming $e^{j\omega t}$ time dependence,

$$\bar{E}(\bar{R}) = \frac{1}{j\omega\varepsilon_o}[\nabla x\bar{H}(\bar{R}) - \bar{J}(\bar{R})] \quad . \tag{4}$$

The integration in Equation (3) is over the source region. Using Equation (1) in Equation (3) gives

$$\bar{H}(\bar{R}) = I_\rho\, \bar{\bar{G}}_{m2}(\bar{R}|\bar{R}')\cdot\hat{\rho} + I_\phi\bar{\bar{G}}_{m2}(\bar{R}|\bar{R}')\cdot\hat{\phi}+I_z\bar{\bar{G}}_{m2}(\bar{R}|\bar{R}')\cdot\hat{z} \quad . \tag{5}$$

The Green's function $\bar{\bar{G}}_{m2}$ is given by Tai [4,5]*:

*Note that, from Equation (1), $\nabla\cdot\bar{\bar{G}}_{m2}=0$ so that only the $\bar{M}$ and $\bar{N}$ vector wave functions are needed in the eigenfunction expansion of $\bar{\bar{G}}_{m2}$.

$$\bar{\bar{G}}_{m2}(\bar{R}|\bar{R}') = \frac{2}{(2\pi-\phi_o)} \int_0^\infty d\lambda \sum_{n=0}^{\infty} \frac{\bar{M}_{o\alpha\lambda}\,\bar{N}'_{o\alpha\lambda} + \bar{N}_{e\alpha\lambda}\,\bar{M}'_{e\alpha\lambda}}{(1+\delta_o)(\lambda^2-k^2)}\,, \tag{6}$$

where $\delta_o = \begin{cases} 1 & n=0 \\ 0 & n\neq 0 \end{cases}$, $\alpha = n\nu = n\,\frac{\pi}{(2\pi-\phi_o)}$; $n=0,1,2\cdots$ and the vector wave functions are*

$$\bar{M}_{\substack{e\\o}\alpha\lambda} = \mp \frac{\alpha}{\rho} J_\alpha(\lambda\rho) \begin{matrix}\sin\\\cos\end{matrix}\alpha\,\phi\,\hat{\rho} - \lambda\, J'_\alpha(\lambda\rho) \begin{matrix}\cos\\\sin\end{matrix}\alpha\,\phi\,\hat{\phi}$$

$$\bar{N}_{\substack{e\\o}\alpha\lambda} = \lambda J_\alpha(\lambda\rho) \begin{matrix}\cos\\\sin\end{matrix}\alpha\,\phi\,\hat{z} \tag{7}$$

Consistent with Tai's notation [4], $\bar{M}'$ and $\bar{N}'$ in Equation (6) refer to $\bar{M}$ and $\bar{N}$ with primed spatial (source) coordinates, whereas elsewhere the prime refers to differentiation with respect to the argument.

In defining field components, superscripts refer to the source polarization and subscripts refer to the field component. Then, from Equation (5-7), $H^\phi_\rho = H^\rho_\rho = H^\phi_\phi = H^\rho_\phi = H^z_z = 0$, and

$$H^\rho_z(\rho,\phi) = \frac{-2I_\rho}{(2\pi-\phi_o)\rho'} \int_0^\infty d\lambda \sum_{n=0}^{\infty} \frac{\alpha\lambda J_\alpha(\lambda\rho)J_\alpha(\lambda\rho')}{(1+\delta_o)(\lambda^2-k^2)} \cos\alpha\phi\sin\alpha\phi' \tag{8}$$

$$H^\phi_z(\rho,\phi) = \frac{-2I_\phi}{(2\pi-\phi_o)} \int_0^\infty d\lambda \sum_{n=0}^{\infty} \frac{\lambda^2 J_\alpha(\lambda\rho)J'_\alpha(\lambda\rho')}{(1+\delta_o)(\lambda^2-k^2)} \cos\alpha\phi\cos\alpha\phi' \tag{9}$$

*The 2-D form of the vector wave functions given above is most easily found from the 3-D form given in Reference [4] by letting h=0.

$$H_\rho^z(\rho,\phi) = \frac{2I_z}{(2\pi-\phi_o)\rho} \int_0^\infty d\lambda \sum_{n=0}^{\infty} \frac{\alpha\lambda J_\alpha(\lambda\rho)J_\alpha(\lambda\rho')}{(1+\delta_o)(\lambda^2-k^2)} \cos\alpha\phi\sin\alpha\phi' \qquad (10)$$

$$H_\phi^z(\rho,\phi) = \frac{-2I_z}{(2\pi-\phi_o)} \int_0^\infty d\lambda \sum_{n=0}^{\infty} \frac{\lambda^2 J'_\alpha(\lambda\rho)J_\alpha(\lambda\rho')}{(1+\delta_o)(\lambda^2-k^2)} \sin\alpha\phi\sin\alpha\phi' \quad . \quad (11)$$

The integrations in Equations (8-10) can be evaluated [4] to give

$$H_z^\rho(\rho,\phi) = \frac{j\pi I_\rho}{(2\pi-\phi_o)\rho'} \sum_{n=0}^{\infty} \frac{\alpha\cos\alpha\phi\sin\alpha\phi'}{(1+\delta_o)} \begin{cases} J_\alpha(k\rho)H_\alpha^{(2)}(k\rho') & \rho<\rho' \\ H_\alpha^{(2)}(k\rho)J_\alpha(k\rho') & \rho>\rho' \end{cases} \qquad (12)$$

$$H_z^\phi(\rho,\phi) = \frac{j\pi k I_\phi}{(2\pi-\phi_o)} \sum_{n=0}^{\infty} \frac{\cos\alpha\phi\cos\alpha\phi'}{(1+\delta_o)} \begin{cases} J_\alpha(k\rho)H_\alpha^{(2)'}(k\rho') & \rho<\rho' \\ H_\alpha^{(2)}(k\rho)J'_\alpha(k\rho') & \rho>\rho' \end{cases} \qquad (13)$$

$$H_\rho^z(\rho,\phi) = \frac{-j\pi I_z}{(2\pi-\phi_o)\rho} \sum_{n=0}^{\infty} \frac{\alpha\cos\alpha\phi\sin\alpha\phi'}{(1+\delta_o)} \begin{cases} J_\alpha(k\rho)H_\alpha^{(2)}(k\rho') & \rho<\rho' \\ H_\alpha^{(2)}(k\rho)J_\alpha(k\rho') & \rho>\rho' \end{cases} \qquad (14)$$

$$H_\phi^z(\rho,\phi) = \frac{j\pi k I_z}{(2\pi-\phi_o)} \sum_{n=0}^{\infty} \frac{\sin\alpha\phi\sin\alpha\phi'}{(1+\delta_o)} \begin{cases} J'_\alpha(k\rho)H_\alpha^{(2)}(k\rho') & \rho<\rho' \\ H_\alpha^{(2)'}(k\rho)J_\alpha(k\rho') & \rho>\rho' \end{cases} \qquad (15)$$

Up to this point the field expressions are completely rigorous.

C. Near Field Calculation

The source and field points are now restricted to be close to the edge of the wedge, so $k\rho<1$ and $k\rho'<1$. Using small argument approximations for the Bessel functions in Equations (12-15) and trigonometric identities yields

$$H_z^{\rho}(\rho,\phi) = \frac{-I_{\rho}}{(2\pi-\phi_0)\rho'} \begin{cases} \frac{1}{2}\sum_{n=1}^{\infty}(\frac{\rho}{\rho'})^{\alpha}[\sin\alpha(\phi+\phi')-\sin\alpha(\phi-\phi')] & \rho<\rho' \\ \frac{1}{2}\sum_{n=1}^{\infty}(\frac{\rho'}{\rho})^{\alpha}[\sin\alpha(\phi+\phi')-\sin\alpha(\phi-\phi')] & \rho>\rho' \end{cases} \quad (16)$$

$$H_z^{\phi}(\rho,\phi) = \frac{I_{\phi}}{(2\pi-\phi_0)\rho'} \begin{cases} \frac{1}{2}\sum_{n=0}^{\infty}(\frac{\rho}{\rho'})^{\alpha}[\cos\alpha(\phi+\phi')+\cos\alpha(\phi-\phi')] & \rho<\rho' \\ \frac{-1}{2}\sum_{n=0}^{\infty}(\frac{\rho'}{\rho})^{\alpha}[\cos\alpha(\phi+\phi')+\cos\alpha(\phi-\phi')]+1 & \rho>\rho' \end{cases} \quad (17)$$

$$H_{\rho}^{z}(\rho,\phi) = \frac{I_z}{(2\pi-\phi_0)\rho} \begin{cases} \frac{1}{2}\sum_{n=1}^{\infty}(\frac{\rho}{\rho'})^{\alpha}[\sin\alpha(\phi+\phi')-\sin\alpha(\phi-\phi')] & \rho<\rho' \\ \frac{1}{2}\sum_{n=1}^{\infty}(\frac{\rho'}{\rho})^{\alpha}[\sin\alpha(\phi+\phi')-\sin\alpha(\phi-\phi')] & \rho>\rho' \end{cases} \quad (18)$$

$$H_{\phi}^{z}(\rho,\phi) = \frac{I_z}{(2\pi-\phi_0)\rho} \begin{cases} \frac{1}{2}\sum_{n=1}^{\infty}(\frac{\rho}{\rho'})^{\alpha}[\cos\alpha(\phi+\phi')-\cos\alpha(\phi-\phi')] & \rho<\rho' \\ \frac{-1}{2}\sum_{n=1}^{\infty}(\frac{\rho'}{\rho})^{\alpha}[\cos\alpha(\phi+\phi')-\cos\alpha(\phi-\phi')] & \rho>\rho' \end{cases} \quad (19)$$

Using the summation formulas A3 and A4 of the Appendix gives, after simplification, the desired closed form results:

$$H_z^{\rho}(\rho,\phi) = \frac{-I_{\rho}\rho^{\nu}\rho'^{,\nu-1}}{2(2\pi-\phi_0)} \left[\frac{\sin\nu(\phi+\phi')}{R_+} - \frac{\sin\nu(\phi-\phi')}{R_-}\right] \tag{20}$$

$$H_z^{\phi}(\rho,\phi) = \frac{I_{\phi}\rho'^{,\nu-1}}{2(2\pi-\phi_0)} \left[\frac{\rho'^{,\nu}-\rho^{\nu}\cos\nu(\phi+\phi')}{R_+} + \frac{\rho'^{,\nu}-\rho^{\nu}\cos\nu(\phi-\phi')}{R_-}\right] \tag{21}$$

$$H_{\rho}^{z}(\rho,\phi) = \frac{I_z\rho^{\nu-1}\rho'^{,\nu}}{2(2\pi-\phi_0)} \left[\frac{\sin\nu(\phi+\phi')}{R_+} - \frac{\sin\nu(\phi-\phi')}{R_-}\right] \tag{22}$$

$$H_{\phi}^{z}(\rho,\phi) = \frac{I_z\rho^{\nu-1}}{2(2\pi-\phi_0)} \left[\frac{\rho'^{,\nu}\cos\nu(\phi+\phi')-\rho^{\nu}}{R_+} - \frac{\rho'^{,\nu}\cos\nu(\phi-\phi')-\rho^{\nu}}{R_-}\right] \tag{23}$$

where $\nu = \frac{\pi}{2\pi-\phi_0}$; $R_{\pm} = \rho^{2\nu}+\rho'^{,2\nu}-2\rho^{\nu}\rho'^{,\nu}\cos\nu(\phi\pm\phi')$.

The $\bar{E}$ fields could be found either by using (4) on (12-15) and applying the procedure of small argument approximations and summation of the series, or using (4) on (20-23) directly. Identical results are obtained with either method for all $\bar{E}$ components except for E_z^z, which would reduce to zero if the curl of (22,23) were taken. Thus, E_z^z is found from (4) and (14-15), while the other $\bar{E}$ components are found using (4) and (20,21). After simplification, $E_z^{\phi} = E_z^{\rho} = E_{\rho}^{z} = E_{\phi}^{z} = 0$, and

$$E_{\rho}^{\rho}(\rho,\phi) = \frac{I_{\rho}\nu(\rho\rho')^{\nu-1}}{2j\omega\varepsilon_0(2\pi-\phi_0)} \left[\frac{2\rho^{\nu}\rho'^{,\nu}-(\rho^{2\nu}+\rho'^{,2\nu})\cos\nu(\phi+\phi')}{R_+^2}\right.$$

$$\left. - \frac{2\rho^{\nu}\rho'^{,\nu}-(\rho^{2\nu}+\rho'^{,2\nu})\cos\nu(\phi-\phi')}{R_-^2}\right] - \frac{I_{\rho}}{j\omega\varepsilon_0\rho}\delta(\rho-\rho')\delta(\phi-\phi') \tag{24}$$

$$E_{\phi}^{\rho}(\rho,\phi) = \frac{I_{\rho}\nu(\rho\rho')^{\nu-1}}{2j\omega\varepsilon_0(2\pi-\phi_0)}\left[\frac{(\rho'^{2\nu}-\rho^{2\nu})\sin\nu(\phi+\phi')}{R_+^2} - \frac{(\rho'^{2\nu}-\rho^{2\nu})\sin\nu(\phi-\phi')}{R_-^2}\right] \tag{25}$$

$$E_{\rho}^{\phi}(\rho,\phi) = \frac{I_{\phi}\nu(\rho\rho')^{\nu-1}}{2j\omega\varepsilon_0(2\pi-\phi_0)}\left[\frac{(\rho^{2\nu}-\rho'^{2\nu})\sin\nu(\phi+\phi')}{R_+^2} + \frac{(\rho^{2\nu}-\rho'^{2\nu})\sin\nu(\phi-\phi')}{R_-^2}\right] \tag{26}$$

$$E_{\phi}^{\phi}(\rho,\phi) = \frac{I_{\phi}\nu(\rho\rho')^{\nu-1}}{2j\omega\varepsilon_0(2\pi-\phi_0)}\left[\frac{2\rho^{\nu}\rho'^{\nu}-(\rho'^{2\nu}+\rho^{2\nu})\cos\nu(\phi+\phi')}{R_+^2}\right.$$

$$\left. + \frac{2\rho^{\nu}\rho'^{\nu}-(\rho'^{2\nu}+\rho^{2\nu})\cos\nu(\phi-\phi')}{R_-^2}\right] - \frac{I_{\phi}}{j\omega\varepsilon_0\rho}\delta(\rho-\rho')\delta(\phi-\phi') \tag{27}$$

From Equations (4,14,15),

$$E_z^z(\rho,\phi) = \frac{-\pi k^2 I_z}{\omega\varepsilon_0(2\pi-\phi_0)}\sum_{n=1}^{\infty}\sin\alpha\phi\sin\alpha\phi'\begin{cases} J_{\alpha}(k\rho)H_{\alpha}^{(2)}(k\rho') & \rho<\rho' \\ -\dfrac{I_z}{j\omega\varepsilon_0\rho}\delta(\rho-\rho')\delta(\phi-\phi') & \\ H_{\alpha}^{(2)}(k\rho)J_{\alpha}(k\rho') & \rho>\rho' \end{cases} \tag{28}$$

Using small argument approximations in the Bessel functions in Equation (28) gives

$$E_z^z(\rho,\phi) = \frac{jk^2 I_z}{2\pi\omega\varepsilon_0}\begin{cases} \displaystyle\sum_{n=1}^{\infty}[\cos\alpha(\phi+\phi')-\cos\alpha(\phi-\phi')]\frac{1}{n}\left(\frac{\rho}{\rho_T}\right)^{\alpha} & \rho<\rho' \\ -\dfrac{I_z}{j\omega\varepsilon_0\rho}\delta(\rho-\rho')\delta(\phi-\phi') & \\ \displaystyle\sum_{n=1}^{\infty}[\cos\alpha(\phi+\phi')-\cos\alpha(\phi-\phi')]\frac{1}{n}\left(\frac{\rho'}{\rho}\right) & \rho>\rho' \end{cases} \tag{29}$$

Using the summation formula (A7) of the Appendix gives

$$E_z^z(\rho,\phi) = \frac{-jk^2 I_z}{4\pi\omega\varepsilon_o} \ell n\left(\frac{R_+}{R_-}\right) - \frac{I_z}{j\omega\varepsilon_o \rho}\,\delta(\rho-\rho')\delta(\phi-\phi') \ . \qquad (30)$$

Equations (20-23), (24-27), and (30) are the complete field expressions for an arbitrary vector electric line source, and are rigorous in the near field limit, including the proper source singularity. Note the proper edge behavior in the fields as $\rho \to 0$. Also note that the expressions for $\overline{H}$ in Equations (20-23) are independent of frequency, indicating a quasi-static result. Hence (20-23) could have been obtained from a conformal mapping approach.

Figure 2 shows the magnitude of E_ϕ^ϕ vs. distance along the surface of the wedge for various wedge angles and λ=1m, ρ'=.1m, ϕ'=0, and I_ϕ=1.

Although the transverse field components are singular at the edge of the ideal wedge, no such singularity exists on any physically realizable electromagnetic scatterer. The reason for this difference is that the ideal wedge has a perfectly sharp edge with a truly discontinuous normal vector, while in physical reality any real "edge" will have a small radius of curvature so that the normal vector at the "edge" will change continuously as it moves around the "edge". This fact was recently used by Rhoads [6] in connection with physically realizable antenna aperture distributions.

Another interesting observation is that some field components become singular when the line source approaches the edge ($\rho' \to 0$). This is in agreement with reciprocity. Of course, this situation could never happen in practice because the perfectly sharp wedge does not exist.

In order to get a feeling for the field behavior at a physical "edge" the mathematically ideal edge of the wedge of this section is removed by adding a circular cylinder tip. Although this geometry is not an exact model of a physical edge, it should allow a qualitative view of the field behavior, with the advantage that it is mathematically tractable.

III. THE CYLINDER TIPPED HALF-PLANE

In this section, using the same method as outlined in Section II, the closed-form field equations for a cylinder tipped wedge are treated. Only the expression for E_ϕ^ϕ for the special case of a half-plane (ϕ_o=0) with a I_ϕ line source (I_z=I_ρ=0) on the surface of the half-plane (ϕ'=0) is presented here, but the general case, for all field components and arbitrary wedge angle, could be developed in the same manner.

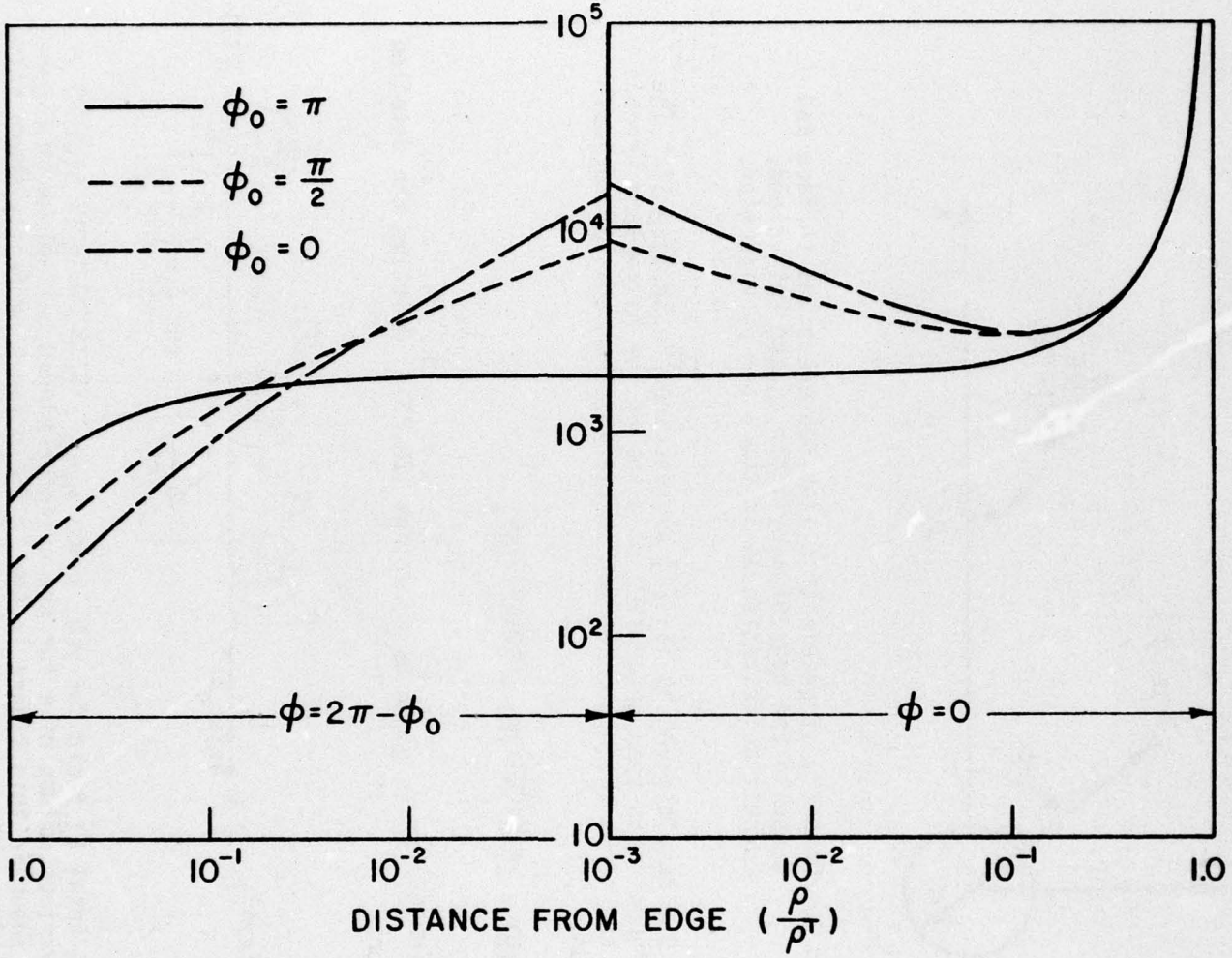

Figure 2. Magnitude of E_ϕ^ϕ (phase=-90°) versus normalized distance along both sides of wedge surface for various wedge angles. ρ'=.1m, λ=1m, ϕ'=0, I_ϕ=1.

The geometry for the cylinder tipped half-plane is shown in Figure 3. The two-dimensional dyadic Green's function may be obtained

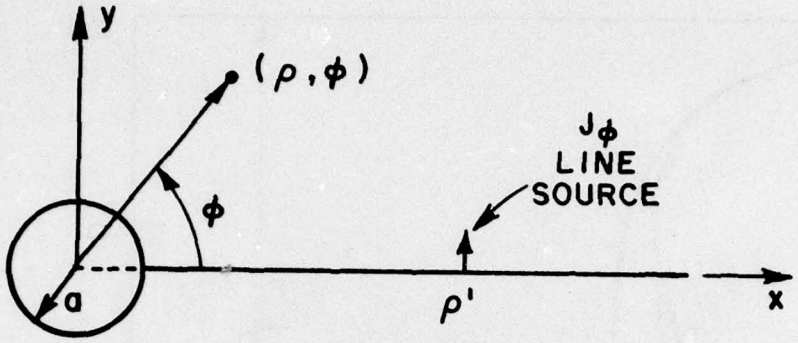

Figure 3. Geometry of an electric line source on the surface and close to the edge of a cylinder tipped half-plane. Current polarization is in the $\hat{\phi}$ (or y) direction.

from the 3-D result given by Tai [4] as described in Section II. The Green's function is seen to consist of a sum of the half-plane Green's function and terms which account for scattering from the cylindrical tip. Thus,

$$\overline{E}^{\phi}(\overline{R}) = \overline{E}^{\phi(\text{wedge})}(\overline{R}) + \overline{E}^{\phi(\text{cyl})}(\overline{R}),$$

where $\overline{E}^{\phi(\text{wedge})}(\overline{R})$ is given by Equations (26,27). Omitting the detailed derivation,

$$E_{\phi}^{\phi(\text{cyl})}(\rho,\phi) = \frac{I_{\phi}}{4\pi j\omega\varepsilon_0\rho\rho'} \frac{\left[\left(\frac{a^2}{\rho\rho'}\right)^{1/2} + \left(\frac{a^2}{\rho\rho'}\right)^{3/2}\right]\cos\frac{\phi}{2} - 2\left(\frac{a^2}{\rho\rho'}\right)}{\left[1-2\left(\frac{a^2}{\rho\rho'}\right)^{1/2}\cos\frac{\phi}{2} + \left(\frac{a^2}{\rho\rho'}\right)\right]^2} \quad (31)$$

The total E_{ϕ}^{ϕ} field for y=0, ϕ'=0, ϕ_0=0, ρ'=.1m, λ=1m is plotted vs. ρ=x for various values of a for the cylinder-tipped half-plane in Figure 4. Also shown in this figure is the E_{ϕ}^{ϕ} field for a perfectly sharp half-plane, which would correspond to a=0 (no cylinder tip). Figure 5 shows the same curves for ρ'=.01 (λ=1m). The ρ=x axis is logarithmic to give an

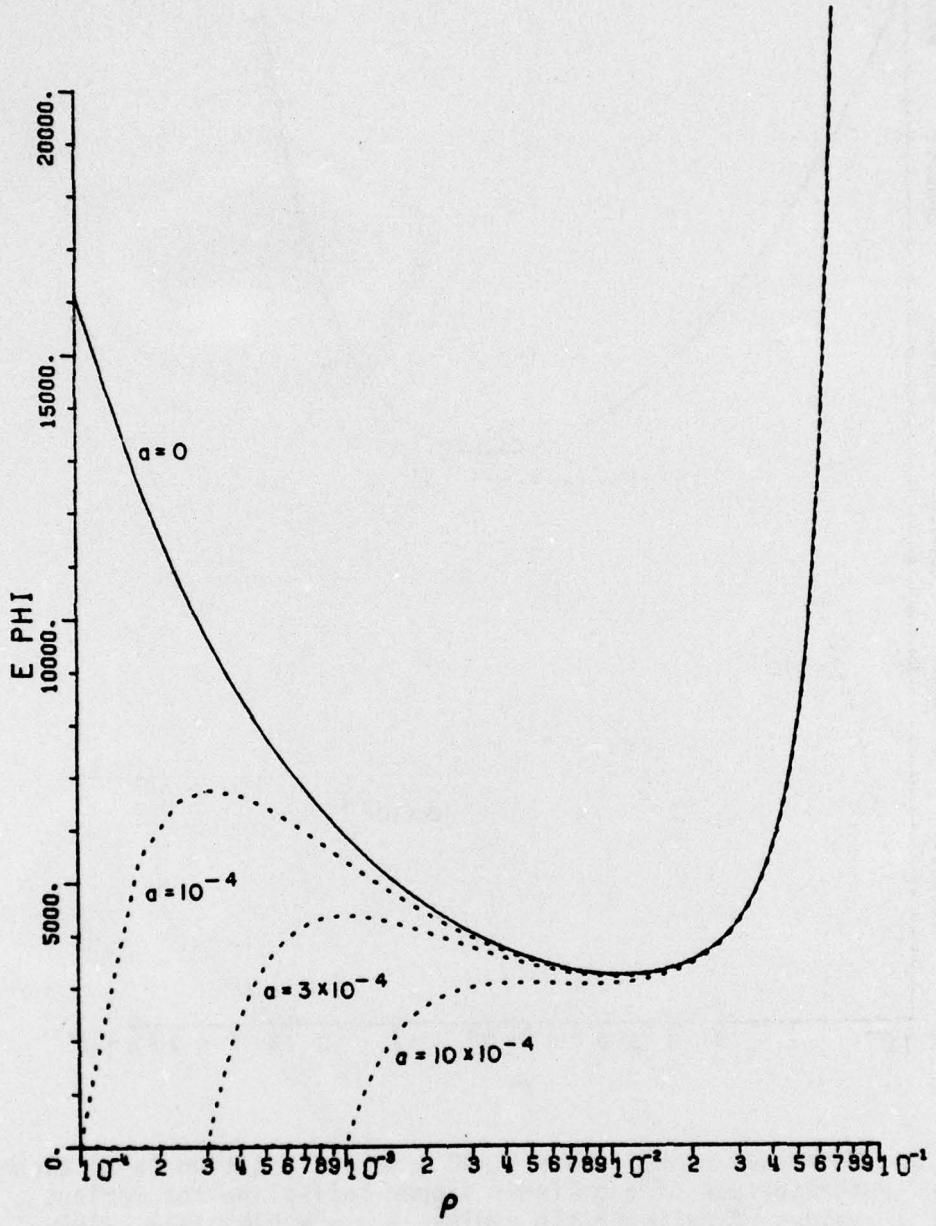

Figure 4. Magnitude of E_ϕ^ϕ (phase = -90°) versus position (ρ=x) along the surface of a cylinder tipped half-plane for various values of cylinder tip radius, a. ρ'=.1m, λ=1m, ϕ'=0, ϕ=0, I_ϕ=1, ϕ_o=0 (half-plane).

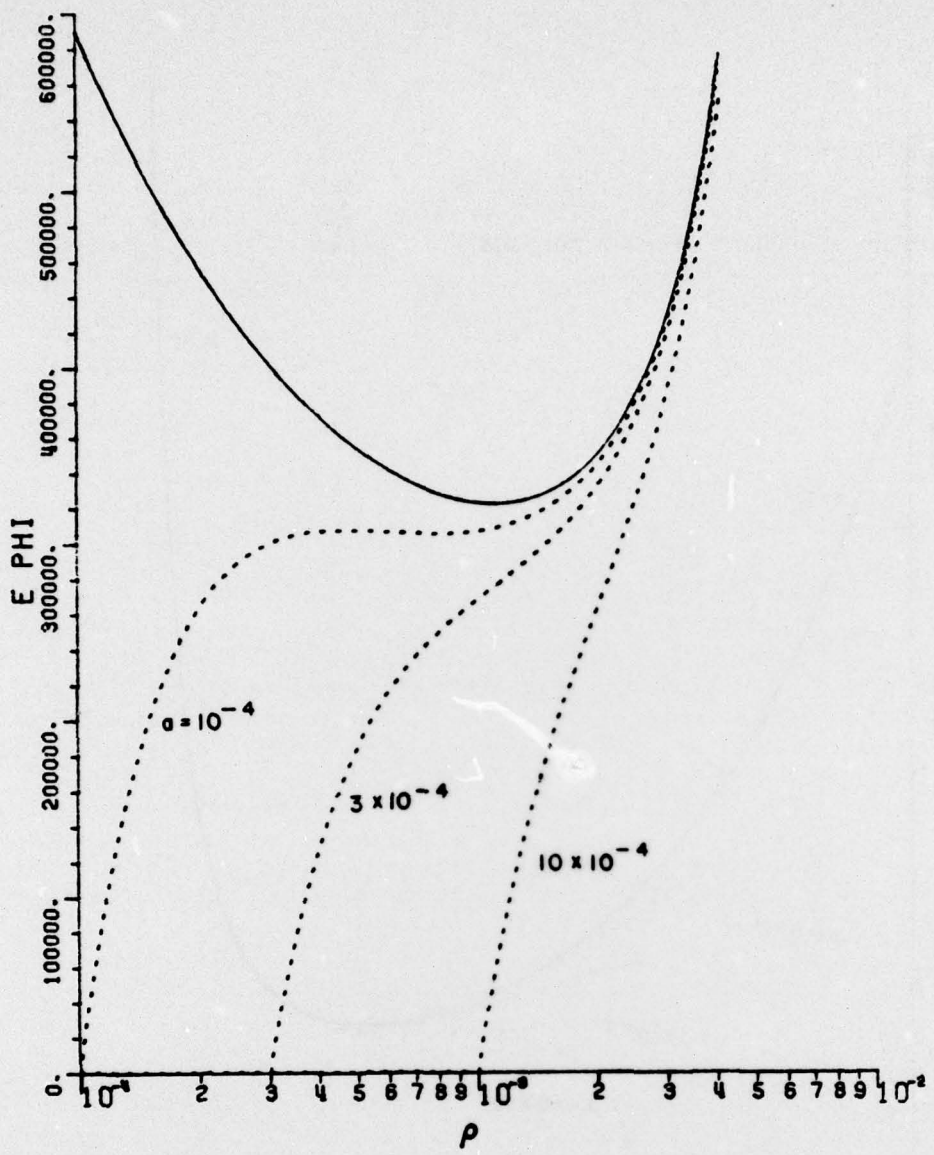

Figure 5. Magnitude of E_{ϕ}^{ϕ} (phase = -90°) versus position (ρ=x) along the surface of a cylinder tipped half-plane for various values of cylinder tip radius, a. ρ'=.01m, λ=1m, ϕ'=0, ϕ=0, I_{ϕ}=1, ϕ_0=0 (half-plane).

expanded view of the edge area. First of all, note that for a=0 (no cylinder) the field is becoming singular as expected. Now, for a small but finite cylinder radius a, the E_ϕ^ϕ field increases as the edge is approached, but reaches a maximum and goes to zero at ρ=a, as required by boundary conditions. It can be seen from Figures 4 and 5 that the field reaches a higher maximum for smaller a, but is not singular except for a=0.

Figure 6 shows the total E_ϕ^ϕ field for y=0, ϕ'=0, ϕ_0=0, ρ'=.1m, λ=1m and a=5x10^{-4}m vs. ρ=x on a rectangular scale for the ideal half-plane and the cylinder-tipped half-plane, along with a sketch of the relative size of the cylinder. Figure 7 shows the same curves for a=5x10^{-5}m.

IV. CONCLUSION

Simple closed form expressions have been derived and presented for an electric line source with arbitrary current flow near and parallel to the edge of a perfectly conducting wedge.

The effect of a physical edge (not perfectly sharp) has been investigated by comparing the fields near the end of a cylinder-tipped half-plane with those near the edge of an ideal half-plane.

The above results indicate that incorporating the singular edge behavior into a solution may not be required to obtain agreement with experiment. However, if one is solving an integral equation based upon the ideal wedge, incorporating the singular edge behavior may improve the stability and convergence of the solution [7].

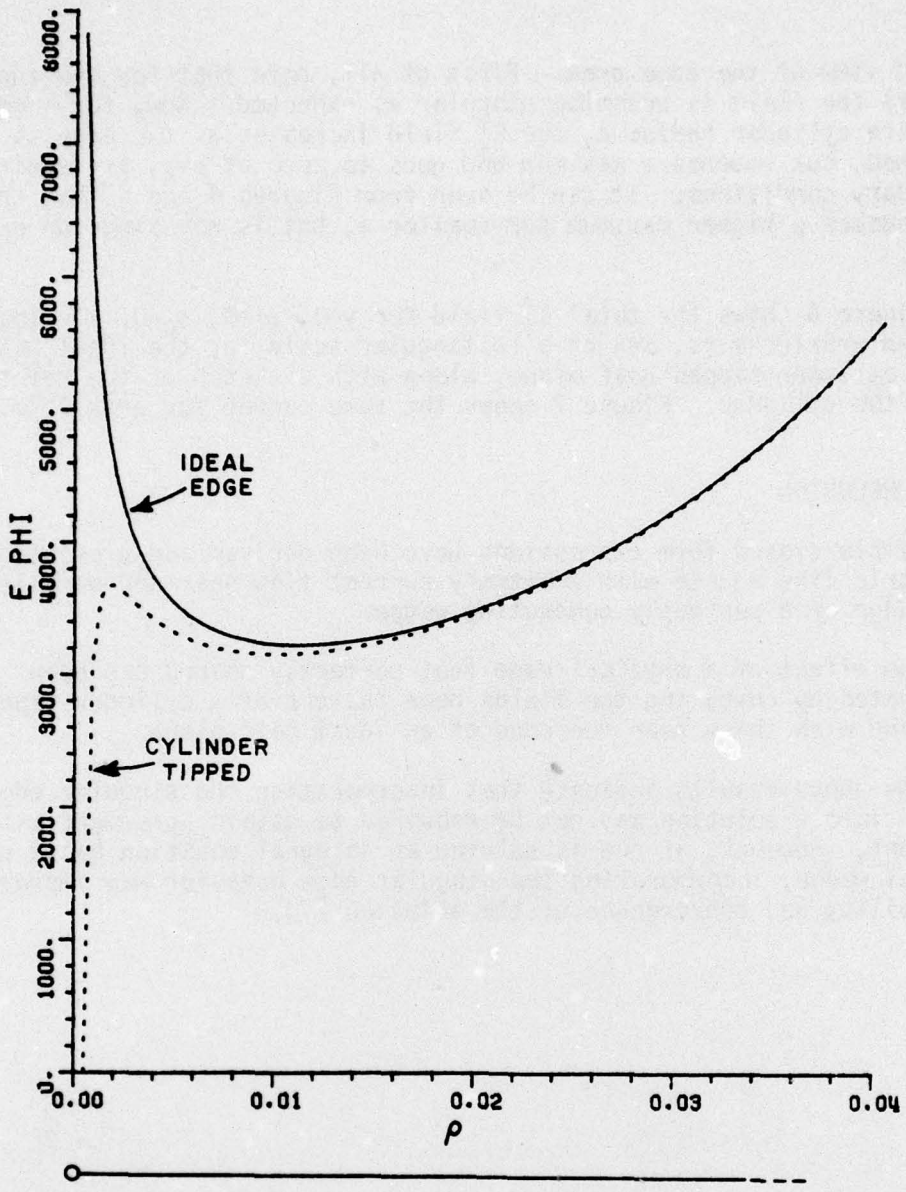

Figure 6. Magnitude of E_{ϕ}^{ϕ} (phase = -90°) versus position (ρ=x) along the surface of a cylinder tipped half-plane compared with that for an ideal half-plane. The relative size of the cylindrical tip is also shown. ρ'=.1m, λ=1m, ϕ'=0, ϕ=0, I_{ϕ}=1, a=ρ'/200.

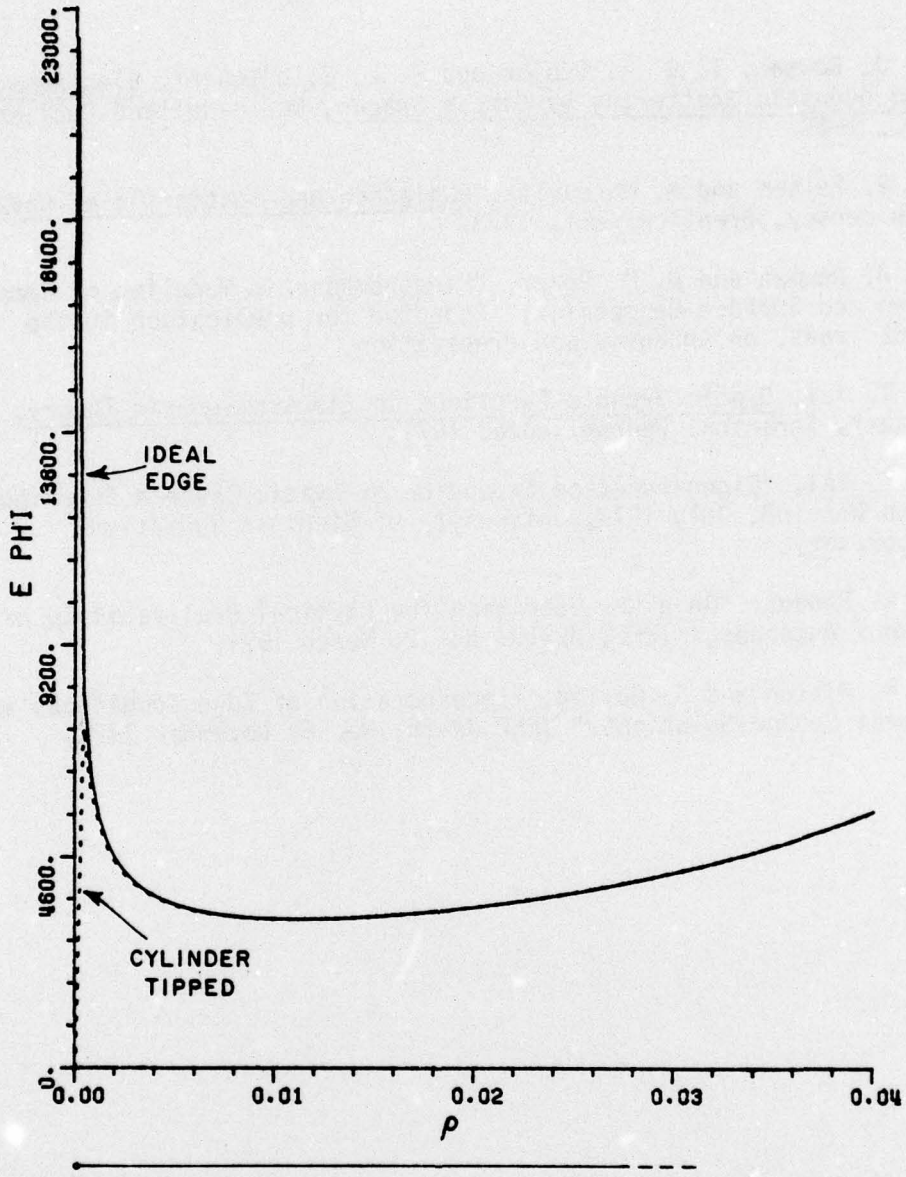

Figure 7. Magnitude of E^{ϕ}_{ϕ} (phase = -90°) versus position (ρ=x) along the surface of a cylinder tipped half-plane compared with that for an ideal half-plane. The relative size of the cylindrical tip is also shown. ρ'=.1m, λ=1m, ϕ'=0, ϕ=0, I_{ϕ}=1, a=ρ'/2000.

REFERENCES

[1] J. J. Bowman, T. B. A. Senior and P. L. E. Uslenghi, Electromagnetic and Acoustic Scattering by Simple Shapes, North-Holland Publishing Co., 1969.

[2] L. B. Felsen and N. Marcuvitz, Radiation and Scattering of Waves, New Jersey, Prentice-Hall, 1973.

[3] E. H. Newman and D. M. Pozar, "Electromagnetic Modeling of Composite Wire and Surface Geometries," Accepted for publication in the IEEE Trans. on Antennas and Propagation.

[4] C. T. Tai, Dyadic Green's Functions in Electromagnetic Theory, Intext, Scranton, Pennsylvania, 1971.

[5] C. T. Tai, "Eigen-Function Expansion of Dyadic Green's Functions," Math Note 28, July 1973, University of Michigan Radiation Laboratory.

[6] D. R. Rhodes: "On a New Condition for Physical Realizability of Planar Antennas," IEEE, AP-19, No. 2, March 1971.

[7] D. R. Wilton and S. Govind, "Incorporation of Edge Conditions in Moment Method Solutions," IEEE AP-25, No. 6, November 1977.

APPENDIX
SUMMATION OF SERIES

Starting with the known result

$$\sum_{n=0}^{\infty} a^{nx} = \frac{1}{1-a^x} \quad ; \qquad x>0,\ 0<a<1 \ , \tag{A1}$$

replace a by $ae^{j\phi}$:

$$\sum_{n=0}^{\infty} a^{nx}\, e^{jn\phi x} = \frac{1}{1-a^x e^{j\phi x}} = \frac{1-a^x e^{-jx\phi}}{1-2a^x\cos(x\phi)+a^{2x}} \ . \tag{A2}$$

Equating real and imaginary parts gives the desired results:

$$\sum_{n=0}^{\infty} a^{nx}\cos(nx\phi) = \frac{1-a^x\cos(x\phi)}{1-2a^x\cos(x\phi)+a^{2x}} \ , \tag{A3}$$

$$\sum_{n=0}^{\infty} a^{nx}\sin(nx\phi) = \frac{+a^x\sin(x\phi)}{1-2a^x\cos(x\phi)+a^{2x}} \ . \tag{A4}$$

Also, from A1,

$$\sum_{n=1}^{\infty} a^{nx} = \frac{a^x}{1-a^x} \ . \tag{A5}$$

Integrating from $-\infty$ to x gives

$$\sum_{n=1}^{\infty} \frac{a^{nx}}{n} = -\ \ell n(1-a^x) \ . \tag{A6}$$

Replacing a by $ae^{j\phi}$ and equating real parts gives

$$\sum_{n=1}^{\infty} \frac{a^{nx}}{n}\cos(nx\phi) = -\ \frac{1}{2}\ \ell n[1-2a^x\cos(x\phi)+a^{2x}] \ . \tag{A7}$$